Shear thinning behavior of aqueous alumina nanoparticle suspensions with saccharides

Katherine A. Ament, Michael R. Kessler, Mufit Akinc
Department of Materials Science and Engineering, Iowa State University, Ames, IA 50011, USA

Abstract

Concentrated aqueous alumina nanoparticle suspensions with addition of low molecular weight saccharides such as fructose, glucose, sucrose, and others were studied by rheometry and low temperature differential scanning calorimetry. The viscosity of the suspensions and melting behaviors of the frozen suspensions were used to develop a model based on particle clustering which describes the viscosity decrease seen with the addition of these saccharides. It appears that characteristics of particle clustering are dependent on the saccharide type and concentration. The proposed model is in qualitative agreement with the observed behavior and the model proposed earlier based on bound water.

Keywords

- A. Suspension;
- Viscosity;
- Alumina;
- Nano particle;
- Saccharide

1. Introduction

Aqueous suspensions of ceramic nanoparticles are frequently used in the production of slip cast, gel cast, and tape cast ceramic components. The non-hazardous nature of water makes it an ideal solvent for ceramic suspensions. Likewise, saccharide molecules are environmentally friendly and biorenewable which is attractive as industry is transitioning toward sustainable technologies.

Aqueous processing of nanosized ceramic particle suspensions poses significant scientific and technological challenges. Due to the decrease in particle size, the specific surface area of these powders is much higher than that of micron or sub-micron sized particles. This provides greater possible contact area for each particle, and consequently interactions with the solvent, other particles, and dispersants become more prominent. The interactions within a ceramic particle suspension are complex. In a given suspension, there are solvent–particle, particle–particle,

solvent–dispersant, and dispersant–particle interactions. Many variables may influence interactions including: pH and ionic strength of the solution, reduction of conformational entropy, solubility and structure of the dispersant, temperature, and electrosteric dispersion to name a few [1].

γ-phase alumina is a metastable transition alumina which is formed during the dehydration of precursor aluminum hydroxides. The surface of nanosized γ-phase powders is highly hydroxylated due to exposure to water vapor. It was postulated by Franks [2] that the OH^- surface groups are primarily singly coordinated due to the presence of many defects, such as plane edges, steps and vacancies, on the powder surface.

The Derjaguin, Landau, Verwey and Overbeek (DVLO) theory describes the interparticle interaction as a sum of the attractive and repulsive forces between particles in suspension. Adsorption of additives, such as saccharides, on the surfaces of particles may promote steric stabilization. Tomasik et al. found that the polysaccharide maltodextrin, a partially hydrolyzed starch, does adsorb onto sub-micron α-alumina and reduces the shear stress at various shear rates [3]. Kim et al. [4] also studied the effect of saccharides on the rheological characteristics of slurries of sub-micron particles and determined that mono- and di-saccharides also adsorb onto alumina with similar results. Li et. al showed that the addition of fructose, sucrose and other polysaccharides to aqueous lowers the viscosity substantially [5] and [6].

The Windhab rheological model [7] shown in Eq. (1) was used to analyze the shear stress as a function of shear rate. This model is particularly powerful in describing the deformation behavior of concentrated suspensions [8]

$$\tau = \tau_0 + (\tau_1 - \tau_0)\left[\left(1 - \exp\left(\frac{-\dot{\gamma}}{\dot{\gamma}^*}\right)\right)\right] + \eta_\infty \dot{\gamma}$$

It incorporates the yield point, τ_0, and the shear stress at the y-axis crossover point, τ_1. The difference between τ_1 and the yield stress τ_0, i.e. ($\tau_1 - \tau_0$), is considered to represent the "shear induced structural change" and $\eta_\infty \eta\infty$ is the slope value of the flow curve at high shear rates. These parameters are all extrapolated from the data. The value of $\dot{\gamma}\square$ is assigned to achieve the best fit (only adjustable parameter). This parameter corresponds to the shear thinning character of the flow curve at low shear rates. The yield point, τ_0 was taken to be the shear stress at the shear rate of 0.5 s^{-1}.

A simple way to compare the viscosity characteristics of a suspension is with the shear rate-dependent viscosity ratio, VR, expressed as $\eta(\dot{\gamma}_1)/\eta(\dot{\gamma}_2)$ where $\dot{\gamma}_2 = 10\dot{\gamma}_1$ [8]. The viscosity ratio (VR) may quantify the dependence of viscosity on shear rate (i.e. shear thinning) behavior of a suspension. The magnitude of the viscosity ratio (VR) is an indicator for the relative degree of shear thinning within a given set of similar suspensions.

The primary purpose of this work is to study the complex behavior of dispersant–particle and solvent–particle interactions through rheometry (specifically viscosity) and low temperature Differential Scanning Calorimetry (DSC) measurements of concentrated suspensions. Water and adsorbed additives at the particle–solvent interface have effects on viscosity [2]. It has been

shown previously that saccharides reduce the viscosity of aqueous alumina nanoparticle suspensions, but the shear thinning character of these suspensions has not been examined in detail.

2. Experimental

2.1. Materials

For this investigation nanosized γ-phase alumina powder with an average particle size of 48 nm (Nanophase Technology Corporation, Burr Ridge, IL) LOT# AAGE1607 was used. The specific surface area and the density of this powder was taken to be 34 m^2/g, and 3.6 g/cm^3 respectively, as stated by the manufacturer. The alumina powders were dried for 2 h at 110°C before use. Typical TEM micrographs of as received alumina powders are shown in Fig. 1.
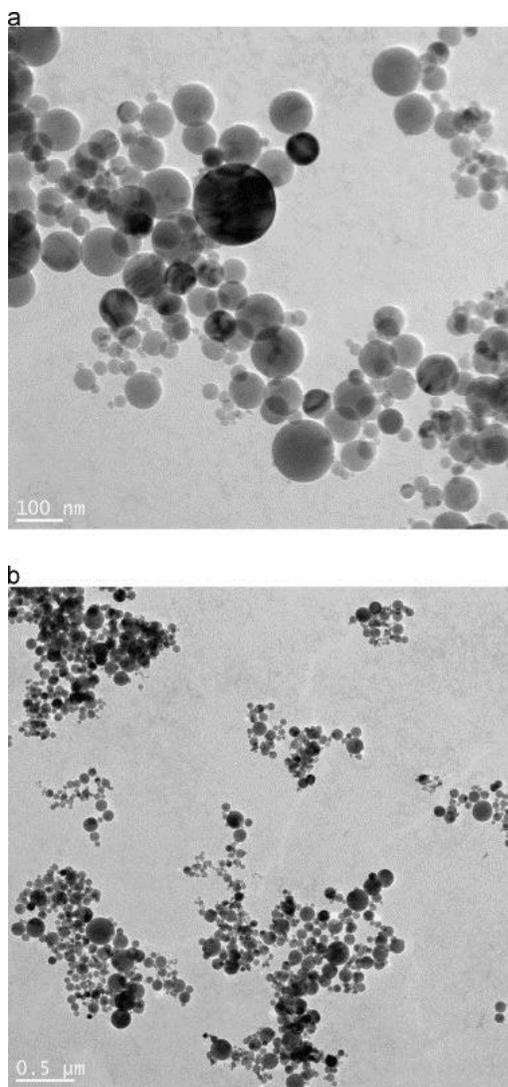

Fig. 1: TEM micrographs of nanosized alumina powder. Nano particles are spherical and show significant variation in size.

Saccharides used in this study were obtained from Sigma-Aldrich (St. Louis, MO) except Methyl α-D glucopyranoside and sucrose which were obtained from Fluka (Distributed by Sigma-Aldrich, St. Louis, MO) and Fisher (Pittsburgh, PA) respectively. Chemical purity of saccharides were as follows: mannitol (98%), sucrose (ACS grade), fructose, glucose, myoinositol, raffinose pentahydrate, methyl α-D glucopyranoside (>99%). The saccharides were used as received, and suspensions were prepared in deionized water.

2.2. Sample preparation and viscosity measurements

Samples were prepared by adding the desired amount of saccharide to deionized water, followed by adding the desired amount of alumina powder to the solution. For example, to prepare a 23 vol% suspension with 10% fructose, 10.8 g of saccharide was added to sufficient water to make a 100 mL fructose solution. To this solution, 108 g of alumina powder (3.6 g/cm^3×30 cm^3=108 g) was added. All samples were shaken with a rocking platform for 24 h to ensure homogeneity before proceeding with rheological measurements.

A Haake RS75 rheometer (Gebrueder Haake GmbH, Karlsruhe, Germany) with a Z40 type cylinder sensor was used for the first set of experiments. The remainder of the experiments was carried out with a TA instruments 2000EX rheometer (New Castle, DE) with a 1° cone and plate sensor and solvent trap. The difference between the data obtained from the two instruments was negligible; hence it is deemed that no distinction is necessary in reporting the data. Experiments were carried out at 25 °C and the sample temperature was maintained with a circulating bath or a Peltier plate. Unless otherwise noted, the shear stress was measured while increasing the shear rate continuously from 0.5 to 500 s^{-1} and back to 0.5 s^{-1} with 10 data points in each decade. The data used for evaluation was the decreasing portion while the increasing shear rate portion was used as a control to ensure reproducible values. At each measurement point, three consecutive measurements were made in 10 s intervals at the specified shear rate and the average viscosity value was reported.

2.3. Differential Scanning Calorimetry (DSC)

A TA Instruments (New Castle, DE) Q2000 differential scanning calorimeter was used to study the melting behavior of frozen aqueous suspensions in order to gain a better understanding of the solvent/particle and saccharide/particle interactions. Suspensions from 16.7 to 41.2 vol% alumina with no saccharide, and suspensions of 28.5 vol% alumina with various saccharides were prepared and approximately 12 mg of each sample was sealed hermetically in an aluminum sample pan. Samples were cooled to −20 °C, held for 1 min and then the temperature was increased at 1 °C/min up to 10 °C.

3. Results and discussion

3.1. Viscosity of suspensions with saccharides

3.1.1. Viscosity of alumina suspensions with no additive

To illustrate the behavior of the alumina water system without additives, a series of suspensions with varying solids contents was measured. It was found that as the solids content is increased in suspensions of 48 nm particles, the viscosity increases. Fig. 2 shows the viscosity as a function of shear rate for suspensions of 16.7–41.2 vol% and illustrates the shear thinning behavior in all samples. Fig. 3 highlights the dramatic increase in viscosity at 100 s^{-1} as the solids content is increased beyond 30 vol%. From 16.7 to 26 vol% there is a modest increase in viscosity, followed by an almost exponential increase from 28.5% to 41.2%. By 33.3 vol% alumina, the mixture loses fluidity and becomes a paste that can still be mixed by shaking. This is in good agreement with the behavior seen in previous work by Li and Akinc [5].
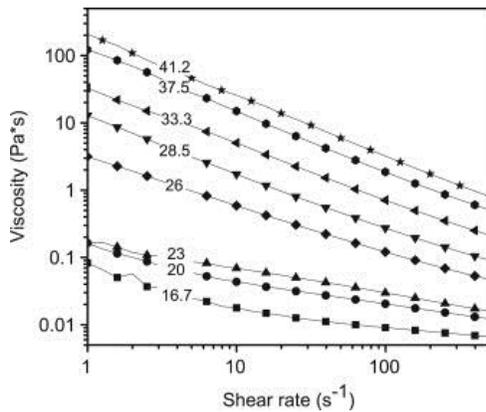

Fig. 2: Viscosity as a function of shear rate for alumina suspensions of various volume percent solids. Data points are taken from the decreasing shear rate branch of the cycle (500–0.5 s^{-1} curve).

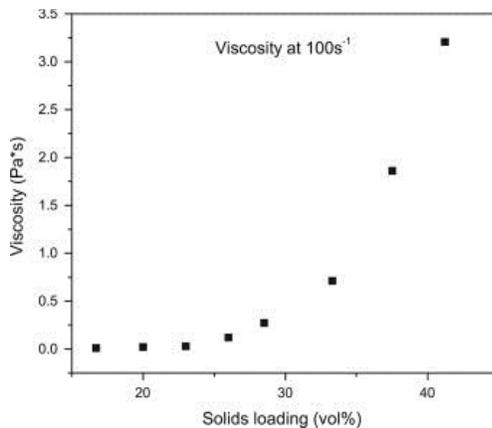Fig. 3: Viscosity at 100 s^{-1} for each suspension of alumina nanoparticles shown in Fig. 2.

3.1.2. Addition of low molecular weight saccharides

For this set of experiments the solid content of the suspensions was kept constant at 23 vol% and the saccharide concentration of 18% by weight of alumina. It was known from previous work of Li and Akinc [5] that 18% fructose would lower the viscosity of the suspension dramatically. Several attempts have been made to explain the mechanism of viscosity reduction of ceramic suspensions by various additives. Tomasik et. al [3] employed a number of low molecular weight compounds like amines, ammonium salts, phenols and carboxylic acids to evaluate the effectiveness as viscosity modifiers for submicron alumina suspensions. They observed a change in pH of suspensions with addition of the additives leading to a statement that the electrostatic interactions are the most dominant ones. However, for the non-dissociating macromolecules, adsorption of these molecules on the particle surface was suggested as the viscosity reduction mechanism. Adsorption of monosaccharides on alumina was also studied by Singh and Mohan [9] and [10]. In a similar study, Bell et al. [11] stated that the molecular size of the monosaccharides is much smaller than the required minimum thickness of 2 nm for steric stabilization. Falkowski et al. [12] showed that there is no shift in the isoelectric point of alumina with the addition of fructose, glucose and their derivatives with carboxylic group attachments which were more effective than fructose indicating that these saccharide derivatives are more potent in displacing water from the alumina surface. Therefore, the viscosity reduction of alumina nano suspensions cannot be explained entirely by either simple electrostatic or steric mechanisms.

Table 1 indicates that all suspensions with or without the additives exhibit shear thinning. Also, each of the additives lowers the viscosity of the suspension, as was reported for fructose previously [5], [6] and [13]. Fructose has the greatest effect, followed by glucose, and sucrose. The viscosity ratio (VR) also shows that the control sample (no saccharide) is most sensitive to shear rate while the sample with fructose is the least affected. This is a manifestation of effectiveness of saccharides as viscosity modifier.

Table 1: Viscosity at selected shear rates and shear rate dependent viscosity ratio (VR) for fructose, glucose, and sucrose containing suspensions at 23 vol% alumina.

Saccharide	Viscosity (mPa s)			VR[a]
	$50\ s^{-1}$	$100\ s^{-1}$	$500\ s^{-1}$	
None	236	157	61	3.87
Sucrose	121	100	48	2.51
Glucose	93	78	40	2.32
Fructose	62	55	33	1.88

a   The viscosity ratio at $50\ s^{-1}$ to $500\ s^{-1}$ shear rate.

3.1.3. Influence of saccharide concentration

The influence of saccharide concentration on the viscosity of 23 vol% alumina suspensions was studied by varying the fructose or glucose concentration from 1% to 18% by weight of dry alumina. Three repetitions of each measurement were made as before, and the data in

consecutive runs were reproducible. The results for fructose and glucose are shown in Fig. 4a and b, respectively.
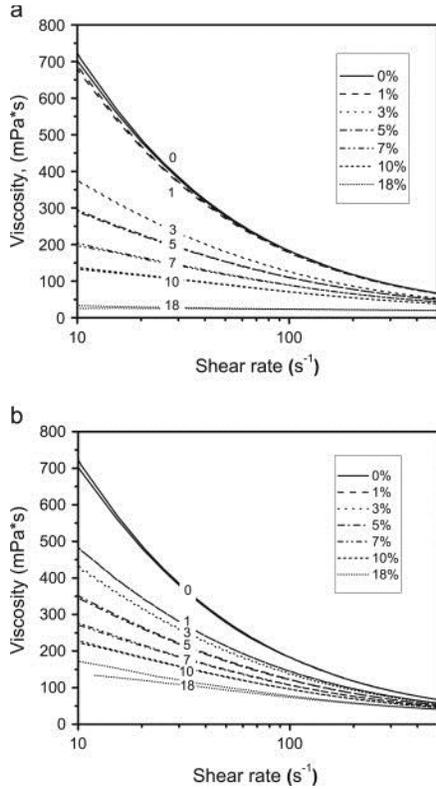

Fig. 4: Variation of viscosity with shear rate for 30 vol% alumina suspensions as a function of (a) fructose and (b) glucose concentration. The pair of curves for each saccharide concentration represents advancing (higher) and decreasing (lower) branches of the viscosity measurement. The coincidence of these curves indicates minimal thixotropy.

First, the hysteresis between advancing and retracting shear rate is negligible. Secondly, the suspension viscosity is decreased as the concentration of the saccharide increases. With increasing saccharide concentration, the behavior of each suspension tends towards Newtonian as the saccharide concentration increases, as indicated by the viscosity ratio in Table 2. With the exception of 1% saccharide addition, fructose is more effective in reducing the viscosity than glucose. Fig. 4a also indicates that the viscosity nearly reaches a limiting value at 18% fructose. It is expected that any additional increase in fructose concentration will produce little or no further reduction in viscosity. This seems reasonable considering it was shown previously through NMR and pyrogenation experiments that, for 30 vol% suspensions, the maximum amount of fructose adsorbed on the particles occurred at a fructose concentration around 15 g/100 g Al_2O_3[6].

Table 2: Viscosity of suspensions of 23 vol% alumina at 50 and 500 s^{-1} and viscosity ratio as a function of fructose concentration.

Alumina nanoparticle suspension viscosities (mPa s)							
% Fructose	50 s⁻¹	500 s⁻¹	VR	% Sucrose	50 s⁻¹	500 s⁻¹	VR
0	278	68	4.12	0	278	68	4.12
1	275	66	4.16	1	214	58	3.70
3	181	53	3.39	3	202	57	3.57
5	154	50	3.22	5	175	53	3.32
7	119	44	2.73	7	150	49	3.07
10	91	39	2.36	10	130	46	2.85
18	62	33	1.88	18	101	41	2.47

Viscosity of 28.5 and 37.5 vol% alumina suspensions with varying amounts of saccharides were also measured. The viscosity of these suspensions decreases as the saccharide loading increases for both glucose and sucrose as in the 23 vol% samples. Higher solids content samples show greater thixotropy, manifested by the difference between the advancing and retracting shear rates. Interestingly, in addition to lowering the viscosity, saccharides also reduce the magnitude of thixotropy. At 100 s^{-1} with the addition of 10 wt% glucose, the magnitude of the thixotropy is reduced from 200 mPa s to 40 mPa s for 37.5 vol% suspension. This phenomenon has been documented previously by Zupanicic [14] who reported that the degree of thixotropy is reduced as Al_2O_3 suspensions are stabilized with polyacrylic acid.

Previously, Kim et. al [4] and Schilling et. al [15] concluded that fructose and sucrose provided the greatest viscosity reduction for aqueous alumina nanoparticle suspensions, while glucose was claimed to be not effective. As shown in Table 1 and Table 3 and Fig. 4, our data clearly indicates that glucose is also effective in lowering the viscosity of the suspension over the whole range of shear rates investigated.

Table 3: Viscosity at 50, 100 and 500 s^{-1} and viscosity ratio as a function of glucose concentration for 37.5 vol% alumina suspensions. Viscosity values are taken from the 500–0.5 s^{-1} branch of the viscosity curve. The high viscosity ratio (VR) indicates shear thinning behavior which decreases with the concentration of glucose.

% Glucose	50 s⁻¹(Pa s)	100 s⁻¹(Pa s)	500 s⁻¹(Pa s)	VRa
0	3.42	1.90	0.54	6.33
3	2.11	1.18	0.35	6.03
5	2.01	1.14	0.34	5.91
10	1.39	0.81	0.26	5.35

a   The viscosity ratio at 50 s⁻¹ to 500 s⁻¹ shear rate.

Sucrose, glucose and fructose are highly hydrated molecules which do not dissociate in water. As the concentration of these sugars increases in an aqueous solution, the viscosity increases [16], but as the concentration of sugar in an alumina nanoparticle suspension increases, the viscosity decreases. Nearly every figure in this paper describing suspensions of alumina nanoparticles shows experimental proof that the greater the concentration of saccharide, the lower the viscosity of the suspension.

3.2. Rheological modeling of shear stress

Suspensions of varying solids contents and a series of 23 vol% suspensions with fructose additions were analyzed with the Windhab model, and fitting parameters for these are given in Table 4 and Table 5. An example fitting of the Windhab model for the 28.5 vol% sample is shown in Fig. 5. The comparison of parameters fit with this model can illustrate the systematic changes within a series of suspensions. In the case of the 23 vol% suspensions, the parameter $\dot{\gamma}^*$ increases with the concentration of fructose. The higher the value of $\dot{\gamma}^*$, the less curvature and the more Newtonian the suspension is. This observation agrees well with the conclusion gathered by the viscosity ratio (VR) values for this set of suspensions. Also, the values for the yield point, y-axis crossover point, slope of flow curve at high shear rates, and shear induced structural change (SISC) decrease with the addition of fructose.

Table 4: Parameters for Windhab model analysis of alumina nanoparticle suspensions and 28.5 vol% suspensions with 5% saccharide.

Saccharide	Vol% alumina	τ_0(Pa)	τ_1(Pa)	$\tau_1-\tau_0$(Pa)	$\dot{\gamma}^*$(s^{-1})	η_∞(Pa s)
None	16.7	0.075	0.139	0.0636	14	0.0077
None	20	0.151	0.458	0.307	14.5	0.0159
None	23	0.114	0.835	0.722	14	0.0215
None	26	2.62	6.701	4.081	8.5	0.0534
None	28.5	11.9	18.47	6.57	9	0.0876
None	33.3	32.07	53.52	21.45	7	0.1755
None	37.5	128.3	153.7	25.4	8	0.3198
None	41.2	207.4	277.8	70.46	10	0.4213
Glucose	28.5	2.392	6.532	4.140	10	0.0618
Sucrose	28.5	2.224	6.713	4.489	10	0.0693
Myoinositol	28.5	3.176	7.263	4.087	9	0.0694
Raffinose pentahydrate	28.5	0.968	4.477	3.509	10	0.0583
Mannitol	28.5	2.214	6.914	4.70	13	0.5986
Methyl-α glucopyranoside	28.5	2.109	6.049	3.941	10	0.05864

Table 5: Windhab model fitting parameters for 23 vol% alumina suspensions with fructose.

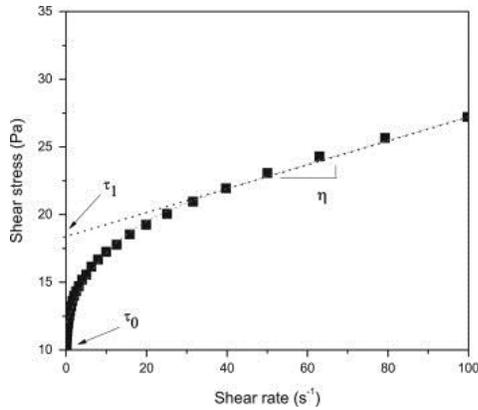| Fructose (wt%)	τ_0(Pa)	τ_1(Pa)	$\tau_1-\tau_0$(Pa)	$\dot{\gamma}^*$(s^{-1})	η_∞(Pa s)
0	0.394	8.646	8.252	9	0.0957
1	0.417	9.182	8.765	10	0.0915
3	0.123	5.414	5.291	11	0.0763
5	0.464	3.935	3.471	14	0.0719
7	0.3834	2.741	2.357	15	0.0625
10	0.2764	1.748	1.471	17	0.0540
18	0.0194	0.209	0.189	20	0.0215

Fig. 5: Fit of the Windhab model (solid line) with data points (symbols) from a 28.5 vol% alumina nanoparticle suspension. The model fit with only one adjustable parameter is excellent with the exception of a slight deviation in the very low shear rate region.

Interestingly, the value for SISC decays exponentially with fructose addition. This implies that as fructose is added to the water/nanoparticle suspension, the degree to which suspension structure is broken up is less with the application of shear stress. It appears that 18% saccharide reduces this value to practically zero.

3.3. Bound water

3.3.1. Free and bound water

In order to study the melting behavior of water as it is altered by its interactions with the alumina surface and the saccharides, a series of DSC experiments were carried out to study the melting behavior of frozen suspensions. DSC curves for aqueous alumina nanoparticle suspensions with solids contents ranging from 16.7 to 41.2 vol% are shown in Fig. 6. The two peaks, free water and bound water, as attributed by Li and Akinc [5] for each curve was fit with a non-linear curve fit tool [17] to find the area, A, under each peak. To calculate the relative amounts of free and bound water, the heat of fusion, ΔH, for free and bound water is needed. Li and Akinc [5] reported that the heat of fusion for bound water is approximately half of that of bulk water. The total water, W_{total}, is related to the enthalpies of both water types by the following equation:

$$W_{total} = W_{free} + W_{bound} = \frac{A_{bound}}{\Delta H_{bound}} + \frac{A_{free}}{\Delta H_{free}}$$

where W, A, and ΔH are mass, area under the DSC peak, and heat of fusion for *free* and *bound* water. The relative fractions of free and bound water were calculated and are shown in Fig. 7. It can be seen in Fig. 7 that as the solids content increases the fraction of bound water increases. At 16.7 vol% solids, the water is mostly free. At this solids content it can be assumed that the free water is filling in the space between particles and the bound fraction, surrounding the particles, melts at a lower temperature than the free water. As the solids content is increased beyond 16.7%, the bound water peak becomes larger and dominates at solids contents greater than 28.5 vol% alumina. Also, as the solids content increases, the bound and free water peaks

converge toward the creation of a single peak spanning across the entire melting range. This indicates that the water bonding environment is becoming more uniform with the addition of very high volume fractions of alumina. Since the particles are expected to have the same influence on the surrounding water molecules, no matter the concentration, the free water must be tending towards the bound water state.
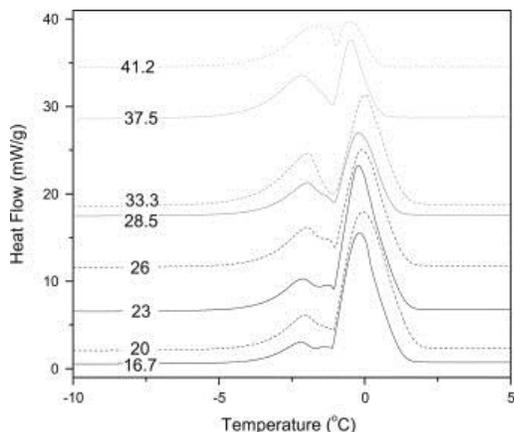

Fig. 6: DSC curves of aqueous alumina nanoparticle suspensions. Samples were heated at a rate of 1 °C/min. The area under each curve is related to the amount of water present in the sample. The curves were shifted vertically for illustration purposes.
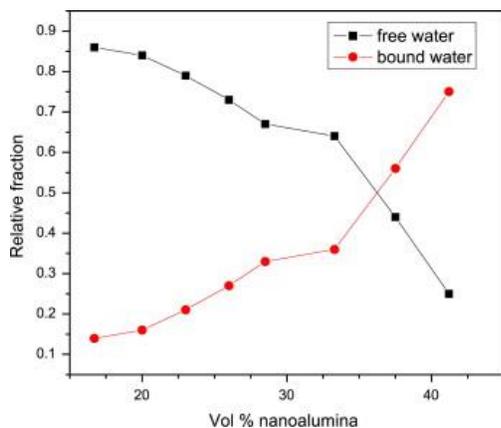

Fig. 7: Fitting the normalized area under the free water peak shows a monotonic increase in bound water with alumina content.

When water freezes, each molecule will hydrogen-bond to form a solid network of ice. During a freezing event in the presence of a surface, the solidification of the hydrogen bonded network of ice is different from its bulk form. Studies of the structure of water in confined environments of nanometer dimensions show that the properties of water are changed at this scale [18]. Previous DSC studies [19], [20] and [21] show that the melting of water entrapped in silica pores occurs at a lower temperature than the bulk water. It is thought that interface ice melting is favored at lower temperatures due to the lower interfacial energy between water and the pore wall than ice and the pore wall [20]. Since both the alumina and silica surfaces are highly hydroxylated, it is

assumed that the cause of interfacial ice melting in alumina suspensions is similar to the mechanism offered for the nanoporous silica/water system.

3.3.2. Melting point depression and peak broadening

The melting point depression for water in the presence of nanometer-scale pores for silica was calculated by Rennie [21] by employing the Kelvin equation. For a 36 nm pore radius, a depression of 1.4 °C was predicted, and for a 20 nm pore radius a depression of 2.5 °C was predicted. As the pore radius decreases, the melting point depression becomes larger. For suspensions containing 16.7–37.5 vol% nanosized alumina, the average temperature shift in the bound water peak was found to be 2.34±0.14 °C which corresponds to a pore radius slightly greater than 20 nm. Since the average particle size for the alumina is 48 nm, an average radius slightly greater than 20 nm is reasonable. The fact that the temperature decrease is similar for all samples suggests that the alumina particle size distribution controls the freezing point depression. Alternatively, one might conclude that the particles form an agglomerated network with pore channels of similar size.

The melting behavior of suspensions with 28.5 vol% alumina and 5 wt% saccharide (based on dry weight of alumina), normalized to be equimolar with glucose, was also investigated. DSC curves in Fig. 6 were also shifted vertically for clarity. It is evident that there are changes in the peak positions, peak shapes, and onset points for the melting of the suspensions with saccharides compared to the reference. The peak positions and shift from the 28.5% alumina suspension reference peak are summarized in Table 6.

The shift of the free water peak to lower temperatures can be explained by freezing point depression (Eq. (3)) caused by the solubility of saccharide molecules in water.

$$\Delta T_f = K_f m_B$$

where ΔT_f is the freezing point depression of the solution relative to the pure solvent, K_f is coefficient of freezing point depression for water and is equal to 1.86 °C/m, and m_B is the molality of sugar, and calculated to be 0.407 mol/kg for 5 wt% saccharide. Knowing that the saccharide molecules do not dissociate appreciably to form ions, freezing point depression predicts a shift of −0.76 °C. The free water peak in each 28.5 vol% suspension follows the freezing point depression rule within±0.4 °C. Mannitol is closest to the predicted value with −0.89 °C reduction in freezing temperature.

The bound water peaks in samples with saccharide show a greater negative deviation than the ones without saccharide. The shift for mannitol and sucrose is approximately −2.0 °C. In addition, presence of saccharides broadens the bound water peak. This could be explained by the modification of the bound water network to create lower energy bonds. The interfacial energy between ice and saccharides near the surface of the alumina particles may be lower than the interfacial energy between ice and the particle surface.

This broadening of the bound water peak was also seen in the work of Li and Akinc [5]. They studied the addition of various concentrations of fructose in 23 vol% alumina by DSC and reported that the bound water peak is reduced with the addition of fructose. But, it appears that the area under the bound water peak was not actually reduced, but the peak was broadened. Due to poor peak shape definition, curve fitting software could not be used to determine the area under the curve. Instead, in order to get a rough estimate of the bound water content, the area was integrated by cutting and weighing the paper under the curve. An average of 3 measurements for each curve was made. For 0%, 3%, 5%, 7%, and 15% fructose, the bound water was estimated to be 0.0213, 0.0125, 0.0217, 0.231, and 0.280 g respectively. Even though the error in these samples is large, clearly, the bound water peak has not disappeared with the addition of fructose. Also, the onset of melting of the bound water is shifted to lower temperatures with increasing saccharide concentration. This phenomenon will be addressed later in the discussion.

Further evidence of peak broadening and shifting is seen in suspensions of 23 vol% alumina with 5% of the various saccharides (see Fig. 8). This indicates that the bound water peak shape is characteristic of the saccharide. It may be due to the characteristics of the OH groups of individual saccharide or even more complex phenomena that cannot be elucidated within the scope of the present study.
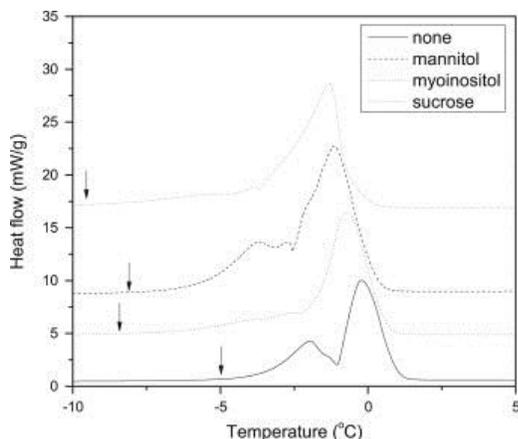

Fig. 8: Melting behavior of 28.5 vol% alumina nanoparticle suspensions with 5 wt% saccharide. Arrows indicate the onset of the bound water peak. The onset was found by extrapolating the zero signal value, found above 2.5 °C, for each curve, and finding its intersection with the heat flow signal.

3.4. Cluster model

It is well known that as the particle size of an oxide powder approaches the nanoscale, the attractive forces between particles become dominant which can lead to particle attraction and agglomeration. Many models have been proposed to describe the characteristics of the agglomeration behavior. Fractal models of colloidal particles are common, and generally well accepted [22] and [23]. Also, models based on particle capture by growing flocs [24] and [25] have been proposed. The proposed model for this system does not contain a lengthy derivation

based on interparticle forces, but instead is a simple geometric model which offers some explanation of the observations made about the alumina nanoparticle system studied in this paper.

Fig. 9 is a simple illustration of the model considered. It consists of primary particles which can aggregate together in one of three packing schemes: simple cubic (SC), body centered cubic (BCC), and face centered cubic (FCC). The primary particles pack together form a primary cluster, and these clusters can interact to form a secondary cluster. Both primary and secondary clusters are assumed to have a spherical boundary surface. It is interesting to note the viscosity increase at 100 s^{-1} for various solids loadings shown in Fig. 3 does correlate to the volume fractions calculated by this simple geometric model. The volume fraction of solids at the point where the space is entirely filled with secondary clusters may be estimated by a simple geometric argument as follows: a single spherical primary particle has a volume of $4/3\pi r^3$, when a primary particle is surrounded by 6 spheres (simple cubic packing) the volume occupied is multiplied by 7. The space occupied by this next coordination ring of radius of 3r is $4/3\pi(3r)^3$. Dividing the occupied space by the total space leads to a solids fraction of 7/27, or 26% solids content. A similar treatment for BCC and FCC packing produces values of 33% and 44% solids. These estimates assume that the secondary clusters fill the entire space.

Volumes

Primary particle:
$7 \times 4/3\pi r^3$

Space enclosing cluster:
$4/3\pi(3r)^3$

Space occupied by particles
In each cluster:
$[4/3\pi(7r^3)]/[4/3\pi(27r^3)]$

SC: 0.26
BCC: 0.33
FCC: 0.44

In each cluster:
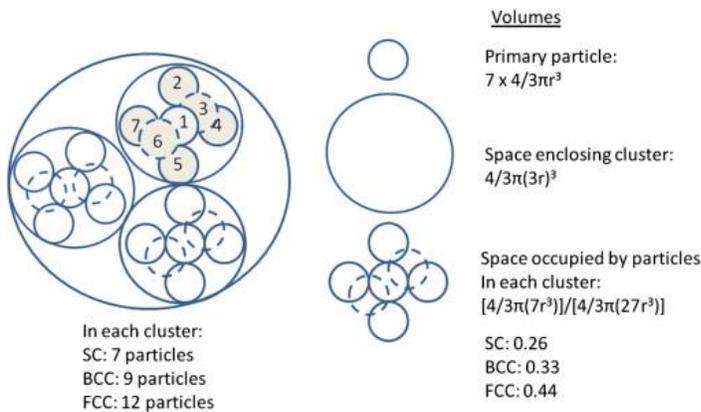SC: 7 particles
BCC: 9 particles
FCC: 12 particles

Fig. 9: Illustration of particle cluster used in the model.

It is possible that at 26 vol% solids (or 33%, or 44%) the secondary clusters of particles become constrained and therefore adopt a higher viscosity. As the solids loading is increased from zero, clusters will form and then become more constrained and entangled, thus increasing the viscosity further. In Fig. 3, it is evident that the viscosity is increased greatly after 28.5 vol% is reached. Any further additions of alumina (33.3–41.2%) would over constrain the clusters and the viscosity will increase sharply.

3.4.1. Cluster breaking

Strong non-Newtonian behavior, especially the existence of yield stress, can be considered an indication of clustering processes [26]. This is manifested in the shear thinning behavior of all suspensions with and without saccharides in this study. There are two important factors in the breakup of clusters in shear flow: kinetic breakup due to shear induced collisions between

clusters and instantaneous breakup due to fluid stresses [27]. Kinetic breakup is reflected in the shear thinning of suspensions with application of shear stress during the measurement process. This process has been shown to be reversible, but time dependent, indicative of a kinetic process. On the other hand, the instantaneous breakup due to fluid stresses is not reversible. Our results suggest that saccharides may play a role in this kind of irreversible change in the suspensions.

3.4.1.1. Kinetic breakup

The values for viscosity as a function of shear rate for all suspensions shown in Fig. 4 were fit with a power law relationship (Eq. (4)) and fitting parameters are shown in Table 4. The equation describing the viscosity of these suspensions is

$$\eta = (\mu_\eta \dot{\gamma})^{-m_\eta}$$

where η is the viscosity at the shear rate $\dot{\gamma}$, μ_η is a constant, and m_η is the exponent. It is no coincidence that the form of this equation is the same as the equation which models the dependence of the maximum aggregate size on the shear rate [28]:

$$r_\infty = \alpha G^{-\beta}$$

where r_∞ r∞ is the maximum aggregate size, α and β are constants, and G is shear rate. It has been shown that the application of stresses will disrupt clusters and is shear rate dependent [24], [26] and [27]. By Eqs. (4) and (5), the reduction in viscosity is proportional to the reduction in cluster size.

There are several characteristics of the viscosity as a function of shear rate that are modified by the addition of saccharides. The constant, μ_η, decreases with increased saccharide as shown in Fig. 10 and Table 7. Mathematically, the constant, μ_η, is the initial value that decays as a function of the independent variable. Therefore, it is reasonable to assume that μ_η reflects the yield value of each suspension. The value of the exponent, m_η, decreases almost linearly with the addition of saccharides as shown in Fig. 11. This constant corresponds to the rate of decay, or the amount of shear thinning experienced by each suspension. This was also reflected in the VR value in Table 2. The value of m for the ripening of $Mg(OH)_2$ and $Fe(OH)_2$ nanoparticles [24] and [27] (~22 nm, and ~43 nm, respectively) was found to be 0.58±0.01, which is very close to the value for the alumina suspension with no saccharide where m=0.57. This provides additional support for the mechanism offered above.
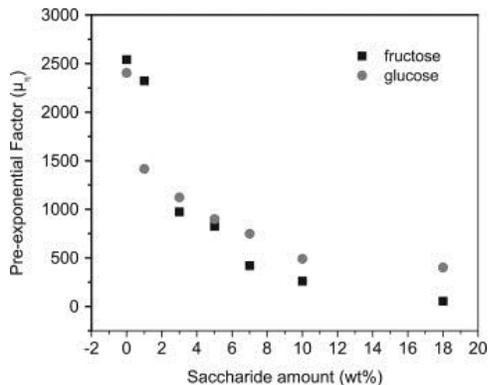

15

Fig. 10: Pre-exponential factor, μ_η, for 23 vol% suspensions with fructose and glucose.
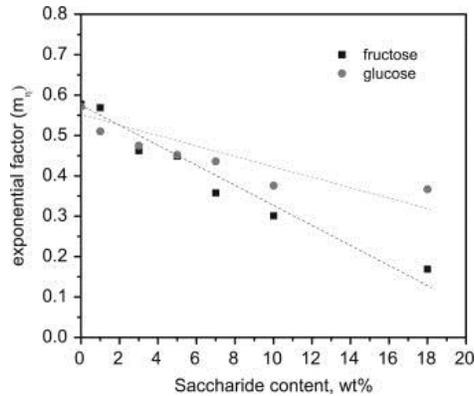

Fig. 11: Variation of exponential factor for 23 vol% suspensions with fructose and glucose concentration (data from Table 7).

3.4.1.2. Instantaneous breakup

Fig. 4a and b shows that as the amount of saccharide in the suspension is increased, the viscosity across all shear rates is decreased. This indicates that there is an irreversible change in the alumina suspension with the addition of saccharide. Even though some of the saccharide is adsorbed onto the particle surface, a significant fraction resides in the solution. This will change the liquid phase characteristics and fluid stresses on the particles, and may initiate instantaneous and irreversible cluster breakup. The clusters may reform as smaller, denser clusters. This can explain how the viscosity of a suspension is dependent on the saccharide amount and is lowered across all shear rates Table 6 and Table 7.

Table 6: Peak temperatures and shifts for 28.5 vol% alumina nanoparticle suspensions with 5 wt% saccharide.

Saccharide	Free water		Bound water	
	Peak temp (°C)	Shift, ΔT_m (°C)	Peak temp (°C)	Shift, ΔT_m (°C)
None	−0.33	–	−1.84	–
Myoinositol	−0.88	−0.55	−2.76	−0.91
Mannitol	−1.22	−0.89	−3.88	−2.04
Sucrose	−1.45	−1.12	−3.99	−2.14

Table 7: Fitting parameters for 23 vol% suspensions with additions of fructose and glucose.

Wt%	Fructose		Glucose	
	μ_η	m_η	μ_η	m_η
0	2540.9	0.578	2404.1	0.571
1	2322.5	0.569	1415.4	0.510
3	973.68	0.462	1123.9	0.475
5	824.43	0.449	898.91	0.452
7	420.54	0.358	748.18	0.436
10	260.08	0.301	491.27	0.376
18	54.889	0.169	400.39	0.367

If the fluid stresses decrease the cluster size and weaken the interactions between clusters, then the suspensions will have a lower viscosity at near zero shear, i.e. lower yield stress which is demonstrated in this study. Due to the initial small size and higher particle density of clusters, it is expected that the suspensions will have lesser shear thinning character since shear stresses will not be able to break up flocs further once the limiting size is reached. This was demonstrated to be true by the VR values reported.

This model fits qualitatively with the previous bound water theory [5] and melting point depression characteristics described above. If the clusters are smaller and denser to begin with, there will be a greater amount of free water in the suspension because a smaller volume of water will be trapped along the particle surface and in interstitial spaces between particles. Also, if the interstitial spaces are becoming smaller with increased saccharide, the melting point depression for bound water will increase which was shown to be the case by the DSC experiments as the onset of the bound water peak was shifted to lower temperatures but did not disappear.

To confirm this hypothesis, it will be necessary to determine the size of alumina nanoparticle clusters in suspension to see if the size decreases with the addition of saccharides and the application of shear. Small angle X-ray Scattering (SAXS) may be useful for elucidation of the cluster size as well [29] and [30].

4. Conclusion

It was shown that the addition of saccharides reduces the viscosity of aqueous alumina nanoparticle suspensions. The viscosity decrease is related to the type of saccharide, and is dependent on the concentration.

The DSC measurements show that saccharides influence the water environment of the suspensions by modifying both the bound and free water, and the melting behavior is dependent on the type of the saccharide molecule employed. Analysis of the viscosity as a function of shear rate for different saccharide concentrations for 23 vol% alumina suspensions by the cluster model indicates that the addition of saccharides affects the cluster size and/or formation which leads to the reduction in viscosity.

Many observed phenomena are supported by the proposed cluster model. The presence of clusters with pore channels is supported by the freezing point depression found in the bound water peaks. If clusters are similar in dimension, this can explain the similar melting temperature

of the bound water peak in suspensions with nanosized alumina particles. It was found that the addition of saccharides lowered the melting point of the bound water which would correspond to the decreased size of pore channels in more closely associated clusters.

References

[1] P.C. Hidber, T.J. Graule, L.J. Gauckler. Influence of the dispersant structure on properties of electrostatically stabilized aqueous alumina suspensions. Journal of the European Ceramic Society, 17 (2–3) (1997), pp. 239–249.

[2] G.V. Franks, Y. Gan. Charging behavior at the alumina–water interface and implications for ceramic processing. Journal of the American Ceramic Society, 90 (11) (2007), pp. 3373–3388

[3] P. Tomasik, Christopher H. Schilling, Ryszard Jankowiak, Jong-Cheol Kim. The role of organic dispersants in aqueous alumina suspensions. Journal of the European Ceramic Society, 23 (2003), pp. 913–919.

[4] J.C. Kim, *et al.* Plasticizing dense alumina slurries with mono- and di-saccharides. Materials Letters, 42 (4) (2000), pp. 221–224.

[5] C. Li, M. Akinc. Role of bound water on the viscosity of nanometric alumina suspensions. Journal of the American Ceramic Society, 88 (6) (2005), pp. 1448–1454.

[6] C. Li, *et al.* Relationship between water mobility and viscosity of nanometric alumina suspensions. Journal of the American Ceramic Society, 88 (10) (2005), pp. 2762–2768

[7] S.T. Beckett (Ed.), Physico-Chemical Aspects of Food Processing, Blackie Academic and Professional, Bishopbriggs, Glasgow (1995).

[8] T.G. Mezger. The Rheology Handbook: For users of rotational and oscillatory rheometers. Vincentz Network GmbH & Co, Hannover, Germany (2006).

[9] K. Singh, S. Mohan. Kinetic studies of the sucrose adsorption onto an alumina interface. Applied Surface Science, 221 (1–4) (2004), pp. 308–318.

[10] K. Singh, S. Mohan. Adsorption behavior of selected monosaccharides onto an alumina interface. Journal of Colloid and Interface Science, 270 (1) (2004), pp. 21–28.

[11] N.S. Bell, M.E. Schendel, M. Piech. Rheological properties of nanopowder alumina coated with adsorbed fatty acids. Journal of Colloid and Interface Science, 287 (2005), pp. 94–106 (Copyright (C) 2012 American Chemical Society (ACS). All Rights Reserved)

[12] P. Falkowski, *et al.* Application of monosaccharides derivatives in colloidal processing of aluminum oxide. Journal of the European Ceramic Society, 30 (14) (2010), pp. 2805–2811

[13] C. Li. Rheological Properties of Aqueous Nanometric Alumina Suspensions. ISU, Ames (2004) (in MSE).

[14] A. Zupancic, R. Lapasin, A. Kristoffersson. Rheological properties of aqueous alpha-Al_2O_3 suspensions: influence of dispersant concentration. Canadian Journal of Chemical Engineering, 77 (4) (1999), pp. 627–636.

[15] C.H. Schilling, *et al.* Rheology of alumina-nanoparticle suspensions: effects of lower saccharides and sugar alcohols. Journal of the European Ceramic Society, 22 (6) (2002), pp. 917–921

[16] J. Mazurkiewicz, P. Tomasik, J. Zaplotny. Relationships between water activity and viscosity of solutions. Food Hydrocolloids, 15 (1) (2001), pp. 43–46

[17] Origin Pro 8, OriginLab Corporation, Northhampton, MA, 2008.

[18] M.C. Bellissent-Funel, J. Lal, L. Bosio. Structural study of water confined in porous glass by neutron scattering. Journal of Chemical Physics, 98 (5) (1993), pp. 4246–4252

[19] E. Levy, *et al.* Structure of water in mesoporous organosilica by calorimetry and inelastic neutron scattering. Surface Science, 603 (1) (2009), pp. 71–77

[20] G.P. Johari. Water's size-dependent freezing to cubic ice. Journal of Chemical Physics, 122 (19) (2005), pp. 194504/1–194504/5.

[21] G.K. Rennie, J. Clifford. Melting of ice in porous solids of the Chemical Society, Faraday Transactions 1: Physical Chemistry in Condensed Phases, 73 (4) (1977), pp. 680–689

[22] R.e.a. Buscall. Scaling Behaviour of the Rheology of aggregate networks formed from colloidal particles. Journal of the Chemical Society, Faraday Transactions 1: Physical Chemistry in Condensed Phases, 84 (12) (1988), pp. 4249–4260.

[23] A.H. Krall, D.A. Weitz. Internal dynamics and elasticity of fractal colloidal gels. Physical Review Letters, 80 (4) (1998), pp. 778–781.

[24] A.A. Potanin. On the mechanism of aggregation in the shear flow of suspensions. Journal of Colloid and Interface Science, 145 (1) (1991), pp. 140–157.

[25] L.B. Brakalov. A connection between the orthokinetic coagulation capture efficiency of aggregates and their maximum size. Engineering Science, 42 (10) (1987), pp. 2373–2383

[26] R.C. Sonntag, W.B. Russel. Structure and breakup of flocs subjected to fluid stresses. II. Theory. Journal of Colloid and Interface Science, 115 (2) (1987), pp. 378–389

[27] R.C. Sonntag, W.B. Russel. Structure and breakup of flocs subjected to fluid stresses. I. Shear experiments. Journal of Colloid and Interface Science, 113 (2) (1986), pp. 399–413

[28] R.K. Chakraborti, *et al.* Changes in fractal dimension during aggregation. Water Research, 37 (4) (2003), pp. 873–883.

[29] L. Li, *et al.* SAXS studies on agglomerative silica suspension under shear. AIP Conference Proceedings, 1027 (2008), pp. 779–781 (Pt. 1, 15th International Congress on Rheology, 2008)

[30] C.A. Kawaguti, *et al.* Small angle X-ray scattering study of surface modified tin oxide nanoparticles prepared by sol–gel route. Journal of Sol–Gel Science and Technology, 37 (3) (2006), pp. 213–217